Improved implementation of the HLL approximate Riemann solver for one-dimensional open channel flows

Xinya Ying & Sam S.Y. Wang F.A.P.

Published online: 26 Apr 2010.

Submit your article to this journal ↗

View related articles ↗

Improved implementation of the HLL approximate Riemann solver for one-dimensional open channel flows

Une meilleure mise en œuvre du solveur approché de Riemann HLL pour les écoulements unidimensionnels dans les canaux à surface libre

XINYA YING, Research Assistant Professor, *National Center for Computational Hydroscience and Engineering*, *The University of Mississippi*, *MS 38677, USA. E-mail: ying@ncche.olemiss.edu (author for correspondence)*

SAM S. Y. WANG, F.A.P., Barnard Distinguished Professor, *National Center for Computational Hydroscience and Engineering*, *The University of Mississippi*, *MS 38677, USA. E-mail: wang@ncche.olemiss.edu*

ABSTRACT

Several new techniques are proposed to overcome the deficiencies in the conventional formulation of the approximate Riemann solvers for one-dimensional open channel flows, which include numerical imbalance and inaccuracy in the solution of discharge. The former arises in the case of irregular geometry and the latter in the presence of a hydraulic jump. These new techniques include: (1) adopting the form of the saint venant equations that include both gravity and pressure in one source term; (2) using water surface level as one of the primitive variables, in stead of cross-sectional area; (3) defining discharge at interface and evaluating it according to the flux obtained by the HLL Riemann solver; and (4) estimating water surface gradient based on piecewise linearly reconstructed variables in the second-order scheme. The performance of the resulting schemes is evaluated by means of theoretical analysis and various test examples, including ideal dam-break flows with dry and wet bed, hydraulic jump, steady flow over bump with hydraulic jump, wave interactions, tidal flow in an open channel, and wave propagation. it is demonstrated that the schemes have excellent numerical balance and mass conservation property and are capable of satisfactorily reproducing various open channel flows.

RÉSUMÉ

On propose plusieurs nouvelles techniques pour surmonter les insuffisances de la formulation conventionnelle des solveurs de Riemann approchés pour les écoulements unidimensionnels en canaux ouverts, insuffisances qui comprennent : un déséquilibre du bilan numérique et une inexactitude du débit calculé. Le premier défaut se produit dans le cas où la géométrie est irrégulière, et le second en présence d'un ressaut hydraulique. Ces nouvelles techniques incluent : (1) l'adoption de la forme des équations de Saint-Venant qui rassemblent la pesanteur et la pression dans un seul terme source ; (2) l'utilisation du niveau de la surface libre, plutôt que de la section transversale, comme l'une des variables primitives; (3) la définition du débit à l'interface et son évaluation par le flux que donne le solveur de Riemann HLL; et (4) l'estimation de la pente de la surface libre sur la base des variables linéaires par morceaux reconstruites dans le schéma du second ordre. La qualité des schémas obtenus est évaluée par une analyse théorique et par divers cas tests, comprenant : les ruptures de barrages sur fond sec et fond humide, le ressaut hydraulique, l'écoulement stationnaire sur une bosse avec ressaut hydraulique, les interactions de vagues, l'écoulement de marée dans un canal ouvert, et la propagation de la houle. On montre que ces schémas ont d'excellentes propriétés de bilan numérique et de conservation de la masse, et sont capables de reproduire d'une manière satisfaisante divers écoulements dans les canaux à surface libre.

Keywords: Open channels, Unsteady flow, HLL Riemann solver, numerical models.

1 Introduction

Modeling open channel flows with discontinuities and mixed flow regimes has been a great challenge to hydraulic researchers and engineers. Although many numerical schemes for open channel flows have been developed, most conventional schemes are often insufficient to handle the flows with discontinuities, mixed flow regimes, and irregular geometry. For example, the four-point implicit scheme which has been widely and successfully used to simulate open channel flows in subcritical flow regime was found to have numerical instability problems in the case of transcritical flows (Jin and Fread, 1997). some schemes produce non-physical oscillation near the steep gradients or discontinuities in

solutions, and artificial viscosity is often required for eliminating non-physical oscillations.

Recently, the applications of Total Variation Diminishing (TVD) schemes and approximate Riemann solvers to one-dimensional open channel flows were frequently reported (e.g., Garcia-Navarro *et al.*, 1992; Garcia-Navarro and Vazquez-Cendon, 2000; Burguete and Garcia-Navarro, 2001; Sanders, 2001; Soares Frazao and Zech, 2002; Delis, 2002; 2003). An in-depth review of TVD schemes and approximate Riemann solvers for the shallow-water equations can be found in the book by Toro (2001). These schemes were originally developed to deal with gas dynamics problems. They are accurate in some situations, but the problems such as numerical imbalance and

non-convergent solution of discharge arise when the channel has complex geometry and the flow includes a hydraulic jump. In conventional formulation, the momentum equation includes three terms that, respectively, represent the hydrostatic pressure force, the pressure force due to cross-sectional variations, and the gravity effect due to bed slope. The numerical imbalance is created when these terms are calculated using different methods, which leads a numerical flow even in a still water test case, as illustrated by Rogers *et al.* (2003) through a two-dimensional simulation of a circular water basin with uneven bathymetry. On the other hand, Delis (2002) evaluated Roe's Riemann solver and several TVD schemes by means of several test cases with a hydraulic jump and revealed that the solution of discharge can not converge at the exact solution over several cells near the hydraulic jump. These limitations restrain the applications of the TVD schemes and approximate Riemann solvers to real-life open channel flows.

So far, many researchers have attempted to overcome these problems. For example, Bermudez and Vazquez (1994) introduced the upwind approach based on local characteristic decompositions for treatment of the source term. Nujic (1995) adopted the form of the governing equation in which the hydrostatic pressure force term is extracted from the flux. Such treatment makes it possible to discretize two source terms using the same method and thus to satisfy the numerical balance. Leveque (1998) developed a wave propagation algorithm by artificially introducing another discontinuity within each computational cell to account for the source terms. Vazquez-Cendon (1999) used an upwind approach for the treatment of the source terms. Garcia-Navarro and Vazquez-Cendon (2000) and Hubbard and Garcia-Navarro (2000) extended the upwind approach to higher-order TVD schemes. Zhou *et al.* (2001) proposed the surface gradient method (SGM) for the treatment of the source terms. In the SGM, water depth at left and right of the interfaces is evaluated based on the linear reconstruction of water surface level. This method can eliminate numerical imbalance problem without introducing a complex algorithm for the source terms. Xu (2002) achieved a well-balanced scheme based on the generalized gas-kinetic BGK model. more Recently, Delis (2003) developed a corrected upwind method to discretize the source term for the HLLE Riemann solver. Rogers *et al.* (2003) used an algebraic approach in which the governing hyperbolic system of conservation laws is reformulated in terms of deviations away from an unforced but separately specified equilibrium state and the numerical balancing is achieved by incorporating the resulting extra physical information. In conclusion, all approaches discussed above can successfully surmount the numerical imbalance. But the problem of inaccuracy in the solution of discharge near a hydraulic jump still remains unsolved, which was clearly illustrated by means of the test cases of steady flows with hydraulic jumps performed by many researchers, such as Zhou *et al.* (2001), Delis (2002, 2003), Xu (2002), and Rogers *et al.* (2003).

In the present study, several new techniques have been adopted in the implementation of the HLL approximate Riemann solvers to overcome the numerical difficulties associated with calculating open channel flows with irregular geometry. The performance of this new approach is demonstrated through various test examples, including ideal dam-break flows with dry and wet bed, hydraulic jump, steady flow over bump with hydraulic jump, wave interactions, tidal flow in an open channel, and wave propagation.

2   Governing equations

One-dimensional unsteady flows in a natural channel with irregular cross-sections are often described by the Saint Venant equations, that is

$$\mathbf{D}\frac{\partial \mathbf{U}}{\partial t} + \frac{\partial \mathbf{F(U)}}{\partial x} = \mathbf{S(U)} \tag{1}$$

where

$$\mathbf{D} = \begin{bmatrix} B & 0 \\ 0 & 1 \end{bmatrix}$$

and B = channel width at water surface elevation (see Fig. 1); $\mathbf{U}$, $\mathbf{F(U)}$, and $\mathbf{S(U)}$ are, respectively, the vectors of primitive variables, fluxes, and sources, defined as follows:

$$\mathbf{U} = \begin{bmatrix} Z \\ Q \end{bmatrix} \quad \mathbf{F(U)} = \begin{bmatrix} Q \\ \frac{Q^2}{A} \end{bmatrix}$$

$$\mathbf{S(U)} = \begin{bmatrix} 0 \\ -gA\dfrac{\partial Z}{\partial x} - g\dfrac{n^2 Q\,|Q|}{R^{4/3}A} \end{bmatrix}$$

In above equations, Z = water surface level; Q = discharge; A = cross-sectional area; g = gravitational acceleration; n = Manning's coefficient; R = hydraulic radius ($= A/P$); and P = wetted perimeter of the channel.

The above form of the Saint Venant equations is commonly used in engineering practice (e.g., Chow, 1959; Cunge *et al.*, 1980; Graf and Altinakar, 1998; Ying *et al.*, 2004). Note that the term $B(\partial Z/\partial t)$ in the continuity equation is equals to $\partial A/\partial t$. In the equation, the driving forces are represented by only one term with the water surface gradient, which makes it very nice for treating the source term because: (1) the variation of water surface is generally much smoother than water depth and bottom and (2) it eliminates the problems such as numerical imbalance that arises due to using different methods to discretize source terms. As a matter of fact, Nujic (1995) proposed a balancing technique in which the pressure term due to water depth is extracted from the flux and combined into the bottom slope term, which actually resulted in a similar form of the governing equation as
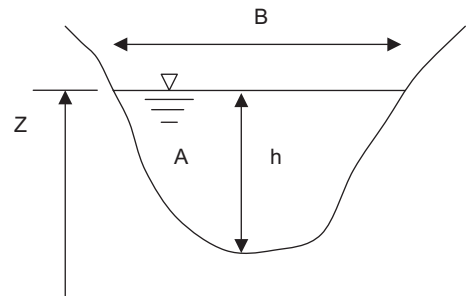

Figure 1   Definition sketch of cross-sectional geometry.

Eq. (1). In addition, it should be pointed out that the adoption of Eq. (1) as the governing equation automatically incorporates the SGM balancing technique (Zhou *et al.*, 2001) into the model formulation.

3   Numerical scheme

The finite volume method is employed for solving the governing equations. Figure 2 shows the computational grid, which has N cells, $N-1$ interfaces between cells and two boundary interfaces.

Integrating Eq. (1) over the ith cell with length of Δx_i yields

$$\mathbf{D}_i \frac{\partial}{\partial t} \int_{\Delta x_i} \mathbf{U}\,dx + \int_{\Delta x_i} \frac{\partial \mathbf{F}(\mathbf{U})}{\partial x}\,dx = \int_{\Delta x_i} \mathbf{S}(\mathbf{U})\,dx \qquad (2)$$

where $\mathbf{D}_i$ represents the mean values of $\mathbf{D}$ over the entire ith cell.

Applying Green's theorem to Eq. (2) and using explicit scheme for time advancing, the following discretized equation is obtained:

$$\mathbf{U}_i^{n+1} = \mathbf{U}_i^n - \frac{\Delta t}{\Delta x_i}\mathbf{D}_i^{-1}\left(\mathbf{F}_{i+1/2} - \mathbf{F}_{i-1/2}\right) + \Delta t \mathbf{D}_i^{-1}\mathbf{S}_i \qquad (3)$$

where $\mathbf{U}_i$ is the vector of primitive variables at ith cell center, representing the average values over the entire cell; $\mathbf{F}_{i+1/2}$ and $\mathbf{F}_{i-1/2}$ are the fluxes at $(i+1/2)$th and $(i-1/2)$th interfaces, (see Fig. 2). According to Godunov (1959), the variables are approximated as constant states within each cell and then the fluxes at interfaces are calculated by solving resultant Riemann problems that exist at interfaces. Here the HLL approximate Riemann solver, proposed by Harten *et al.* (1983), is used to calculate the intercell flux, because of its robustness and ease to implement. The HLL scheme assumes only one constant intermediate state between the left wave and the right wave, as shown in Fig. 3. The intercell flux is defined as

$$\mathbf{F}_{\text{HLL}} = \begin{cases} \mathbf{F}_L & \text{when } S_L \geq 0 \\ \mathbf{F}^* & \text{when } S_L < 0 < S_R \\ \mathbf{F}_R & \text{when } S_R \leq 0 \end{cases} \qquad (4)$$

where S_L and S_R are left and right wave speeds, respectively, (see Fig. 3). That is, the flux at an interface is determined by the left state if $S_L \geq 0$ (Fig. 3a), and by the right state if $S_R \leq 0$ (Fig. 3c).
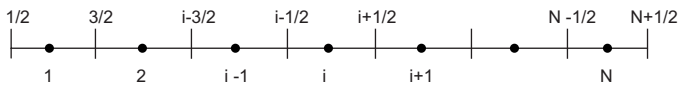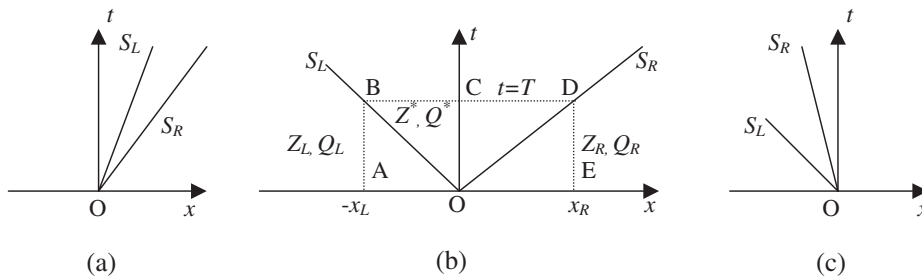
When $S_L < 0$ and $S_R > 0$ (Fig. 3b), the Harten–Lax–Van Leer approach provides the approximate expression for estimating $\mathbf{F}^*$.

Using a standard operator-splitting approach (Toro 1992; Fraccarollo and Toro 1995), the full governing equation (1) can be split into two equations: the equation including source term and the following homogeneous equation:

$$\mathbf{D}\frac{\partial \mathbf{U}}{\partial t} + \frac{\partial \mathbf{F}(\mathbf{U})}{\partial x} = 0 \qquad (5)$$

Let f_1 and f_2 are two components of the flux $\mathbf{F}$, that is, $\mathbf{F} = [f_1, f_2]^{\text{T}}$. Equation (5) can be rewritten as

$$\frac{\partial A}{\partial t} + \frac{\partial f_1}{\partial x} = 0 \qquad (6)$$

$$\frac{\partial Q}{\partial t} + \frac{\partial f_2}{\partial x} = 0 \qquad (7)$$

Applying Eq. (6) on the control volume OABC and OCDE (see Fig. 3b), respectively, gives

$$x_L(A_L^* - A_L) = T(f_1^L - f_1^*) \qquad (8)$$

$$x_R(A_R^* - A_R) = T(f_1^* - f_1^R) \qquad (9)$$

where f_1^* and f_2^* are two components of the flux $\mathbf{F}^*$, that is, $\mathbf{F}^* = [f_1^*, f_2^*]^{\text{T}}$.

Note that

$$S_L = -\frac{x_L}{T} \quad S_R = \frac{x_R}{T}$$
$$A_L^* - A_L = (Z^* - Z_L)B_L \quad A_R^* - A_R = (Z^* - Z_R)B_R.$$

The latter two relationships are generally accepted as valid approximations if the variation of water surface level is small. Substituting these relationships into Eqs (8) and (9), we obtain

$$-S_L(Z^* - Z_L)B_L = (f_1^L - f_1^*) \qquad (10)$$

$$S_R(Z^* - Z_R)B_R = (f_1^* - f_1^R) \qquad (11)$$

Eliminating Z^* from Eqs (10) and (11) gives

$$f_1^* = \frac{S_R B_R f_1^L - S_L B_L f_1^R + S_L B_L S_R B_R(Z_R - Z_L)}{S_R B_R - S_L B_L} \qquad (12)$$

As a matter of fact, for a prismatic channel with rectangular cross-section and horizontal bottom in which $B_L = B_R$, Eq. (12) becomes the same form of the conventional HLL scheme (Fraccarollo and Toro, 1995).

Figure 2   Definition sketch of computational grid.

Figure 3   Three possible wave configurations.

Applying Eq. (7) on the control volume OABC and OCDE (see Fig. 3b), respectively, gives

$$x_{\text{L}}(Q^* - Q_{\text{L}}) = T(f_2^{\text{L}} - f_2^*) \tag{13}$$

$$x_{\text{R}}(Q^* - Q_{\text{R}}) = T(f_2^* - f_2^{\text{R}}) \tag{14}$$

Substituting $S_{\text{L}} = -(x_{\text{L}}/T)$ and $S_{\text{R}} = x_{\text{R}}/T$ into Eqs (13) and (14), and then eliminating Q^*, we can obtain

$$f_2^* = \frac{S_{\text{R}} f_2^{\text{L}} - S_{\text{L}} f_2^{\text{R}} + S_{\text{L}} S_{\text{R}}(Q_{\text{R}} - Q_{\text{L}})}{S_{\text{R}} - S_{\text{L}}} \tag{15}$$

The wave speeds S_{L} and S_{R} are estimated according to the following equations:

$$S_{\text{L}} = \min\left(V_{\text{L}} - \sqrt{g\bar{h}_{\text{L}}}, V^* - \sqrt{g\bar{h}^*}\right) \tag{16}$$

$$S_{\text{R}} = \max\left(V_{\text{R}} + \sqrt{g\bar{h}_{\text{R}}}, V^* + \sqrt{g\bar{h}^*}\right) \tag{17}$$

where V_{L} and V_{R} are velocities of the left and right states, respectively; $\bar{h}_{\text{L}}$ and $\bar{h}_{\text{R}}$ are averaged water depth of the left and right states, which is defined according to $\bar{h} = A/B$,

$$V^* = \frac{1}{2}(V_{\text{L}} + V_{\text{R}}) + \sqrt{g\bar{h}_{\text{L}}} - \sqrt{g\bar{h}_{\text{R}}} \tag{18}$$

$$\sqrt{g h^*} = \frac{1}{2}\left(\sqrt{g\bar{h}_{\text{L}}} + \sqrt{g\bar{h}_{\text{R}}}\right) + \frac{1}{4}(V_{\text{L}} - V_{\text{R}}) \tag{19}$$

Note that for a dry bed problem the wave speeds S_{L} and S_{R} are estimated according to the following expressions:

$$S_{\text{L}} = V_{\text{L}} - \sqrt{g\bar{h}_{\text{L}}} \quad S_{\text{R}} = V_{\text{L}} + 2\sqrt{g\bar{h}_{\text{L}}} \quad \text{for right dry bed} \tag{20}$$

$$S_{\text{L}} = V_{\text{R}} - 2\sqrt{g\bar{h}_{\text{R}}}, \quad S_{\text{R}} = V_{\text{R}} + \sqrt{g\bar{h}_{\text{R}}} \quad \text{for left dry bed} \tag{21}$$

The HLL approximate Riemann solver discussed above is a first-order scheme. The second-order spatial accuracy can be obtained through a piecewise linear reconstruction of primitive variables in each cell, which leads to

$$\mathbf{U}_{i+\frac{1}{2}}^L = \mathbf{U}_i + \frac{\Delta x_i}{2}\left(\frac{\partial \mathbf{U}}{\partial x}\right)_i \tag{22}$$

$$\mathbf{U}_{i+\frac{1}{2}}^R = \mathbf{U}_{i+1} - \frac{\Delta x_{i+1}}{2}\left(\frac{\partial \mathbf{U}}{\partial x}\right)_{i+1} \tag{23}$$

To avoid numerical oscillations, proper slope limiters must be used in estimating the slope $\partial \mathbf{U}/\partial x$. Here, the minmod limiter is adopted due to its robustness. Therefore, the slope in the ith cell can be expressed by

$$\left(\frac{\partial \mathbf{U}}{\partial x}\right)_i = \text{minmod}\left(\frac{\mathbf{U}_i - \mathbf{U}_{i-1}}{x_i - x_{i-1}}, \frac{\mathbf{U}_{i+1} - \mathbf{U}_i}{x_{i+1} - x_i}\right) \tag{24}$$

The minmod function is defined as the argument with smaller value if all arguments have the same sign and otherwise it is zero.

The source terms in Eq. (3) include the water surface gradient term and the friction term. The simplest and commonly used approach for estimating the water surface gradient is the centered difference scheme, that is,

$$\left(\frac{\partial Z}{\partial x}\right)_i = \frac{Z_{i+1} - Z_{i-1}}{x_{i+1} - x_{i-1}} \tag{25}$$

For the second-order scheme, using Eq. (25) may produce non-monotone solutions near shocks in some cases such as the idealized dam-break problem with wet bed. Therefore, we propose a new method to estimate the water surface gradient for the second-order scheme, as expressed by

$$\left(\frac{\partial Z}{\partial x}\right)_i = \frac{\bar{Z}_{i+1/2} - \bar{Z}_{i-1/2}}{\Delta x_i} \tag{26}$$

where $\bar{Z}_{i+1/2} = (Z_{i+1/2}^L + Z_{i+1/2}^R)/2$ and $\bar{Z}_{i-1/2} (Z_{i-1/2}^L + Z_{i-1/2}^R)/2$ are, respectively, the average water surface levels at the right and the left interface of ith cell. It is important to note that although Eq. (26) is also a centered scheme, it relates the water surface gradient to the piecewise linearly reconstructed water surface level. This can make the numerical scheme more consistent in representing the driving forces and the fluxes, as both are estimated based on the piecewise linearly reconstructed variables. Improvement in the numerical solution by using Eq. (26) is demonstrated by means of the idealized dam-break problem with wet bed (see Appendix). The numerical tests also show that the proposed scheme with Eq. (26) works well even in the case of non-uniform grid.

The friction term is explicitly evaluated based on the pointwise method. Therefore, the values of Z and Q at next time can be obtained by solving Eq. (3) explicitly. Such a method is often referred to as the cell centered scheme as both variables Z and Q are defined at cell centers. For convenience, hereafter this scheme is referred as the HLL-A scheme. However, the solution of the discharge from such a numerical scheme may be not accurate in the event that there is a hydraulic jump, as shown in the numerical tests that follow.

To find a solution to this problem, let us first look at the discretized Eq. (3). For clarity, the continuity equation in Eq. (3) is rewritten as

$$Z_i^{n+1} = Z_i^n - \frac{1}{B_i}\frac{\Delta t}{\Delta x_i}\left[(f_1)_{i+1/2} - (f_1)_{i-1/2}\right] \tag{27}$$

It is important to note that in the discretized continuity equation, the variable Q is replaced by the flux f_1. Therefore, it is obvious that the continuity equation only ensures the conservation property of the flux f_1, instead of discharge Q. Let us take a steady flow as an example. When the solution converges at steady state, (i.e., $Z_i^{n+1} = Z_i^n$), from the continuity Eq. (27), we can see that the flux f_1 has the same value at all interfaces, which is equal to the inflow discharge or the flux f_1 at inflow boundary. In other words, the flux f_1 has the exact conservation property, while the discharge Q calculated by the momentum equation is not ensured to have such property. For this reason, we choose the values of flux f_1 as the solution of discharge, while the values of Q_i calculated by Eq. (3) are only used to define the constant states of the Riemann problems. The resulting scheme is called the HLL-B scheme.

The solution procedures for the proposed schemes are summarized below:

(1) Performing piecewise linear reconstruction of primitive variables in each cell according to Eqs (22)–(24). Note that this step is required only for the second-order scheme.
(2) Calculating wave speeds according to Eqs (16) and (17) or Eqs (20) and (21).
(3) Evaluating fluxes by Eqs (4), (12) and (15). For the HLL-B scheme, discharge Q is evaluated based on $Q = f_1$.
(4) Obtaining the values of Z and Q at cell centers at next time from Eq. (3). For the HLL-A scheme, these values are considered as the solutions of Z and Q. For the HLL-B scheme, only the values of Z are used as the solution, while the values of Q are provisional and only used to define the Riemann problems at next time.

It should be noted that the solution procedures for both HLL-A and HLL-B schemes are essentially identical. The only difference between two schemes is the approaches used to evaluate discharges. In the HLL-A scheme, discharges are estimated in conventional way, that is, according to the momentum equation, while in the HLL-B scheme discharges are assumed to be equal to the values of flux f_1. For this reason, the both schemes give the same results of water level Z.

It is easy to see that the resulting schemes do not cause numerically generated flow or numerical imbalance problem. Let us consider an open channel filled with water at rest. Obviously, the water will remain at rest if no disturbance is applied to the domain and boundaries. If we apply the above schemes to simulate this case, we can see the source terms, including water surface gradient term and friction term, and flux terms in Eq. (3) are exactly equal to zero at initial time, no matter how bottom and cross-section change. As a result, the solutions of Z and Q at succeeding times will remain the same as initial state, in other words, no flow is numerically generated.

Like most explicit schemes, the schemes discussed above are subject to the Courant–Friedrichs–Lewy stability condition, that is

$$N_{\text{CFL}} = \text{Max}\left[\frac{\Delta t}{\Delta x_i}(|V_i| + \sqrt{gA_i/B_i})\right] \leq 1 \quad 1 \leq i \leq N$$

(28)

4   Boundary conditions and dry bed treatment

For control volume method, boundary conditions are often treated by introducing ghost cells. In these ghost cells, primitive variables and their gradients are specified. In the event that inflow is subcritical, discharge is often specified at the ghost cell and water level is evaluated by extrapolation based on the values of two adjacent interior cells. For supercritical inflow, both discharge and water level are specified at the ghost cell and gradient of water level is set to zero. At open outflow boundary, both discharge and water level at the ghost cell are calculated by linear extrapolation based on the values of two adjacent interior cells. For the outflow boundary with specified water level, the water

level at the ghost cell is set to the specified value. This approach to treat boundary conditions is common and often sufficient for control volume method (Sanders, 2001).

Channel flows may occur over initially dry areas. The commonly used approach to deal with this problem is to define a sufficiently small water depth and zero velocity at dry nodes, so that the dry domain can be computed in the same way as wet part without introducing significant error.

5   Numerical tests

Seven test examples are selected to examine the performance of the proposed schemes. Examples 1 and 2 are idealized dam-break problems in a rectangular channel with dry bed and wet bed, respectively. Example 1 is designed to examine the performance of the numerical scheme when the wave has very shallow front edge. In example 2, the solution has a right traveling surge and a depression wave that moves upstream. Example 3 examines the scheme's capability to deal with hydraulic jump, that is, the transition from supercritical flow to subcritical flow. Example 4 is a steady flow over a bump, which examines the numerical balance and the convergence of numerical solution to a steady state in the presence of transcritical flows and bottom elevation changes. Example 5 is designed to test the scheme's ability to capture wave interactions. Example 6 is selected to test the scheme's ability to reproduce the time-dependent tidal flow in an open channel. Example 7 examines numerical scheme's ability to capture short wave propagation in the shallow water.

5.1   Idealized dam-break problem in a rectangular channel with dry bed

Consider a 1200-m long channel with rectangular cross-section, which is assumed to be horizontal and frictionless. A dam is located at 500 m from upstream end of the channel. Initially, upstream water depth is 10 m and downstream channel is dry. This is an ideal dam-break example and has been widely used for testing numerical schemes (e.g., Zoppou and Roberts, 2003; Ying *et al.*, 2004). In the computation, $\Delta x = 10$ m, $\Delta t = 0.1$ s, and initial water depth in the downstream channel was specified as 10^{-7} m.

The numerical and exact solutions of water depth h, discharge Q, and velocity V at 30 s after the dam failure are presented in Fig. 4 (a–c), respectively. The exact solutions can be found in the books by Henderson (1966) and Toro (2001). Note that the HLL-A scheme results in the same results as the HLL-B scheme for this example in terms of water depth h, discharge Q, and velocity V. Therefore, in Fig. 4 only results from the HLL-B schemes are presented. Fig. 4 shows that both the first-order and the second-order schemes result in overall reasonable solutions, which have no entropy violation. As expected, the first-order scheme is more diffusive than the second-order scheme.

Figure 4(c) reveals that the solutions of velocity are slightly under-predicted near the wave front edge. In fact, most of numerical schemes cannot accurately predict velocity near the wave
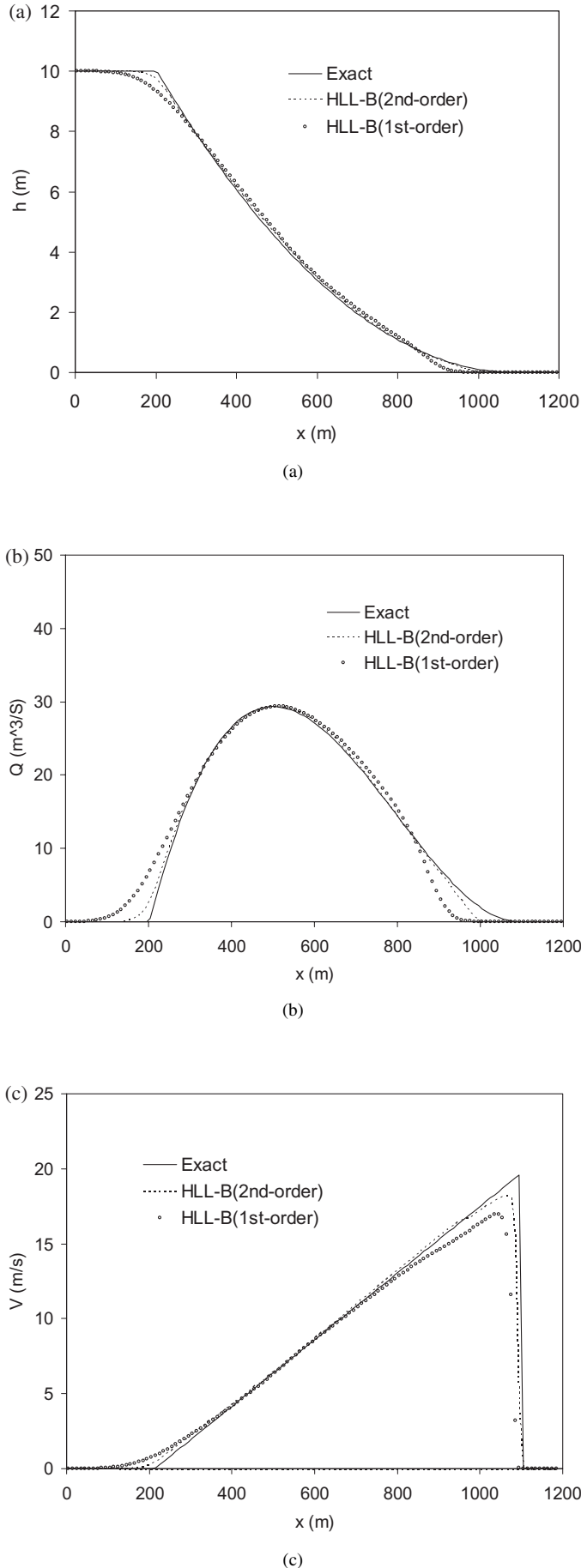
(a)

(b)

(c)

Figure 4 Comparison of numerical solutions with analytic solutions for the dam-break problem with dry bed at $t = 30$ s: (a) water depth; (b) discharge; and (c) velocity.

front edge for dry bed dam-break problem, because of very small water depth in the area. For example, Sanders (2001) reported that the Roe-type Riemann solver with MUSCL approach predicted velocity with significant under-prediction or over-prediction near the front edge, which is strongly dependent on the selection of N_{CFL}. It should be noted that this insufficiency only results in very limited influence on the flow, which can be observed from the numerical solutions of water depth and discharge, as shown in Fig. 4(a) and (b), respectively. Further tests demonstrate that the solutions by the present schemes are almost independent of N_{CFL}, that is, no significant difference in solutions is observed by using different time step as long as N_{CFL} is kept less than one.

5.2 Idealized dam-break problem in a rectangular channel with wet bed

In this test example, the initial downstream water depth is 2.0 m and other computational conditions are the same as in Example 1. This example is selected for assessing the performance of the numerical scheme when the solution has a surge or shock wave. In the computation, the cell size $\Delta x = 10$ m and time step $\Delta t = 0.1$ s were used.

Figure 5 shows the numerical and exact solutions of water depth h, discharge Q, and velocity V at 30 s after the dam failure. It is observed that both first-order scheme and second-order scheme are capable of well predicting the essential characteristics of the flow, such as front location, height of the shock wave, discharge, and velocity. However, the first-order scheme produces more diffusive solutions near the discontinuities than the second-order scheme.

5.3 Hydraulic jump in a rectangular channel

Whenever flow regime changes from supercritical flow to subcritical flow, the water surface rises abruptly and a hydraulic jump occurs. In this section the proposed scheme is applied to simulate such a common hydraulic phenomenon. The predicted results are compared with the experimental data measured in a 14.0-m-long and 0.46-m-wide metal flume with horizontal bottom (Gharangik and Chaudhry, 1991). At the upstream boundary, water depth is 0.031 m, velocity is 3.831 m/s, and corresponding Froude number is 7.0. Water depth at downstream end is 0.265 m. In the computation the channel was discretized by 47 cells. The time step was 0.05 s. Initial water depth and velocity over the entire channel was assumed to be the same as those at the upstream boundary. The water depth at the downstream boundary was increased from 0.031 to 0.265 m in 50 s and maintained until a steady hydraulic jump was formed. Value of the Manning's coefficient $n = 0.0085$ s/m$^{1/3}$ was used, which was determined by matching experimental data with simulation results and is within the range of 0.008 to 0.011, as suggested by the experiment.

Figure 6(a) shows that the location of the hydraulic jump is predicted by both the first-order and the second-order schemes with satisfactory accuracy. The numerical results show that the hydraulic jump is formed in 2 cells for the second-order scheme and 3 cells for the first-order scheme. It should be noted that the
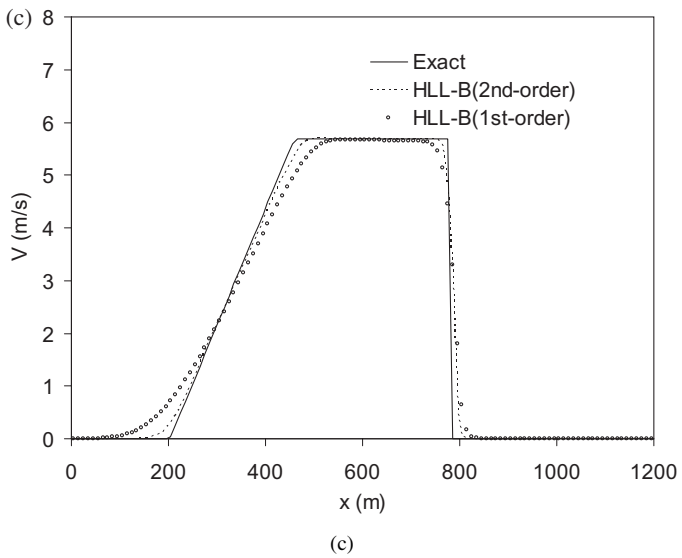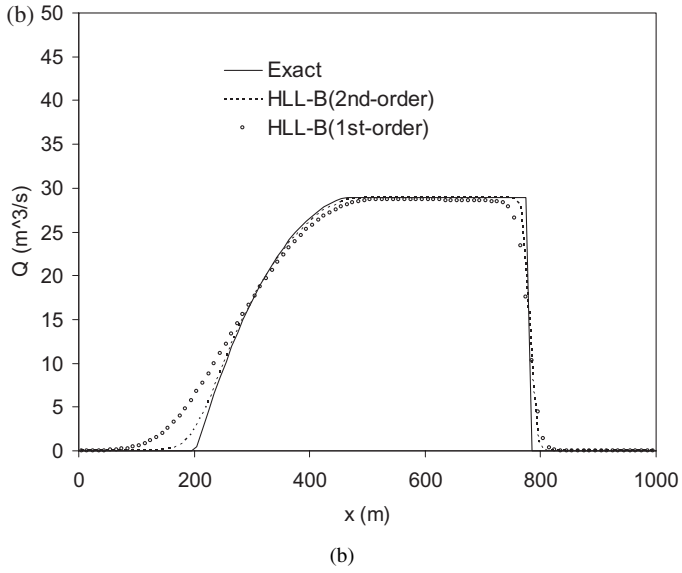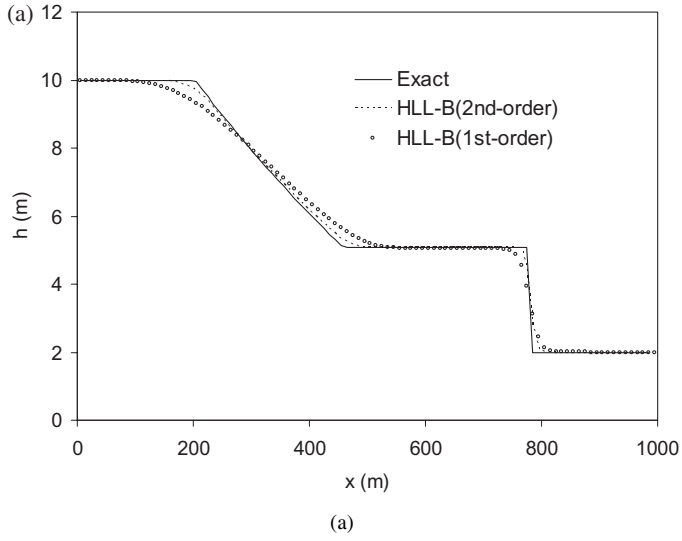
(a)

(a)

(a)

(a)

(b)

(b)

(b)

(b)

(c)

(c)

(c)

(c)

Figure 5 Comparison of numerical solutions with analytic solutions for the dam-break problem with wet bed at $t = 30\,\text{s}$: (a) water depth; (b) discharge; and (c) velocity.
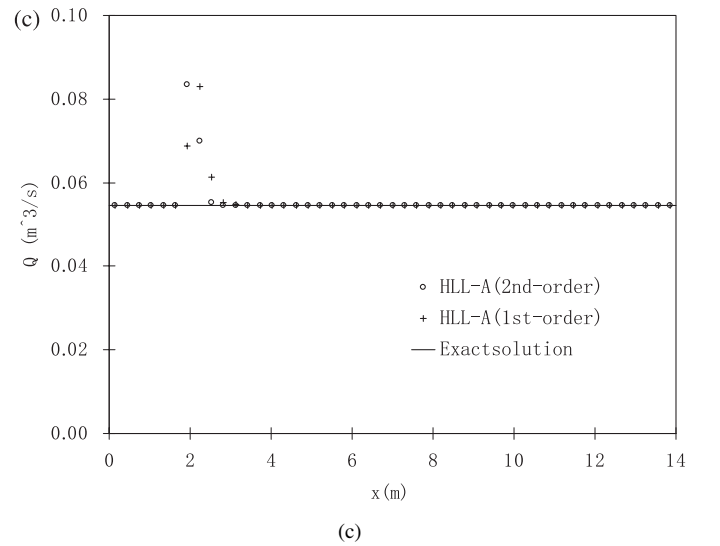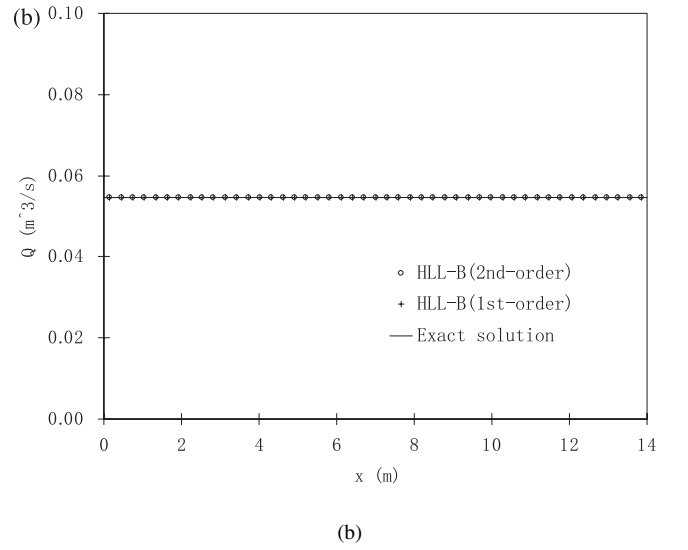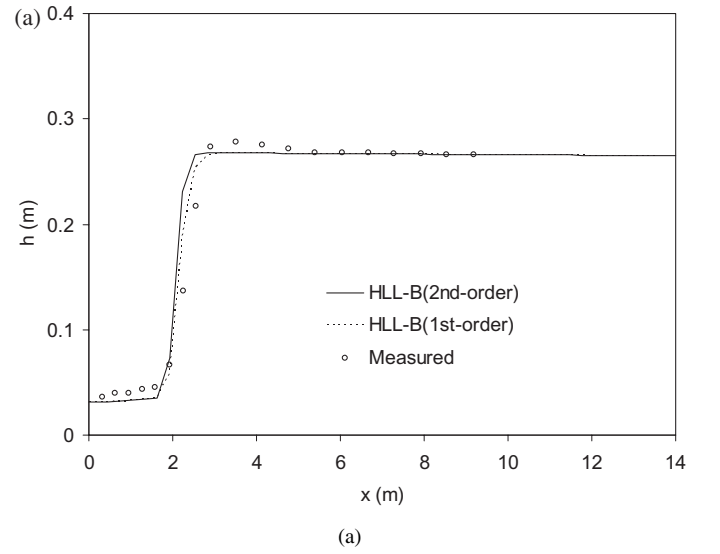
Figure 6 Comparison of numerical solutions with experimental data or analytic solution for the hydraulic jump test case: (a) water depth; (b) discharge predicted by HLL-B schemes; and (c) discharge predicted by the HLL-A schemes.

shallow-water model is incapable of accurately predicting the water surface profile of hydraulic jumps, as it does not represent the dominant physical processes involved in a hydraulic jump such as surface roller. Therefore, the performance of the schemes cannot be measured by comparing predicted surface profile to the measured data, because the former depends on the cell size of the computational grid. For this reason, Fig. 6(a) does not indicate that the first-order scheme has superiority in performance over the second-order scheme in the case of hydraulic jumps.

The numerical solutions of discharge along channel from the HLL-B scheme and the HLL-A scheme are presented in Fig. 6(b) and (c), respectively. Since it is steady flow, the discharge should keep constant along the entire channel length according to the law of mass conservation. From Fig. 6(b), it is observed that the solutions from the HLL-B schemes can converge at the exact solution. The difference between numerical solutions from the HLL-B schemes and the exact value of discharge ($= 0.054\,6\text{m}^3/\text{s}$) along the entire channel length is indistinguishable. Figure 6(c) shows the solutions from HLL-A schemes cannot converge at the exact solution over 2 or 3 cells near the hydraulic jump. It should be noted that such inaccuracy in the solution of discharge was a longstanding problem and was reported by many researchers in their simulations of steady flow over bump test case (e.g., Vazquez-Cendon, 1999; Hubbard and Garcia-Navarro, 2000; Zhou *et al.*, 2001; Xu, 2002; Delis, 2003; Rogers *et al.*, 2003). The results from this test case demonstrate that the HLL-B scheme can successfully eliminate the problem and accurately predict the discharge even in the presence of hydraulic jumps.

5.4 Steady flow over a bump

Consider a 1-m-wide and 25-m-long channel with rectangular cross-section. The channel bed is assumed to be horizontal and frictionless. Bottom elevation Z_b is defined by

$$Z_b = \begin{cases} 0 & x < 8 \text{ and } x > 12 \\ 0.2 - 0.05(x - 10)^2 & 8 \le x \le 12 \end{cases}$$

The downstream boundary condition of $Z = 0.33\,\text{m}$ and the inflow condition of $Q = 0.18\,\text{m}^3/\text{s}$ were imposed in the computation. This test case was widely used to study the convergence of numerical solutions to a steady state (e.g., Vazquez-Cendon, 1999; Zhou *et al.*, 2001; Valiani *et al.*, 2002).

The analytic solution for this test case was obtained by the Bernoulli equation and the location of hydraulic jump was determined by the conservation of momentum across the jump. In the computation the grid size was the same as used in the numerical simulation by Valiani *et al.* (2002), that is, $\Delta x = 0.1\,\text{m}$, so that the computed results from the present scheme can be compared with the existing results. The time step $\Delta t = 0.01$ was used.

Figure 7(a) shows that the numerical solution of water level is in good agreement with the analytic solution. Particularly, the location of the hydraulic jump is accurately predicted. Figure 7(b) indicates that the solution from the HLL-B scheme has excellent conservation property and the difference between predicted and exact discharge is indistinguishable. The results from this
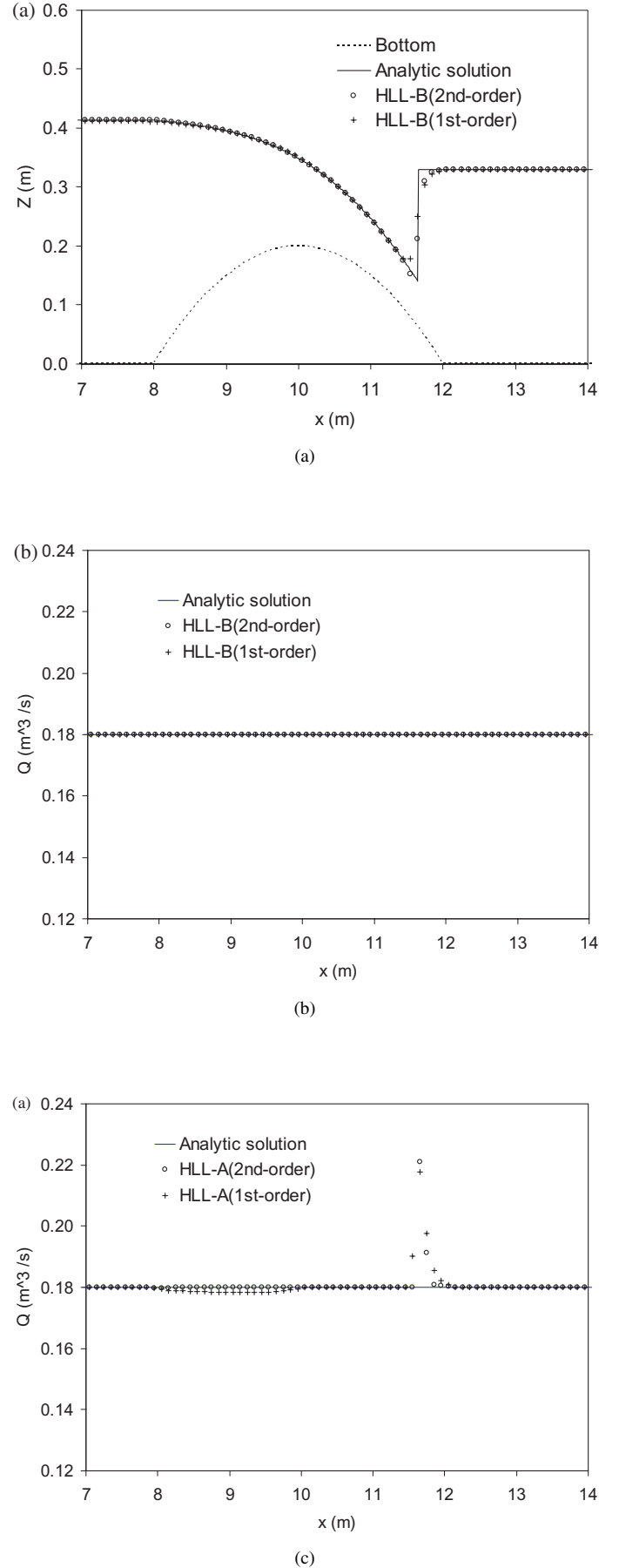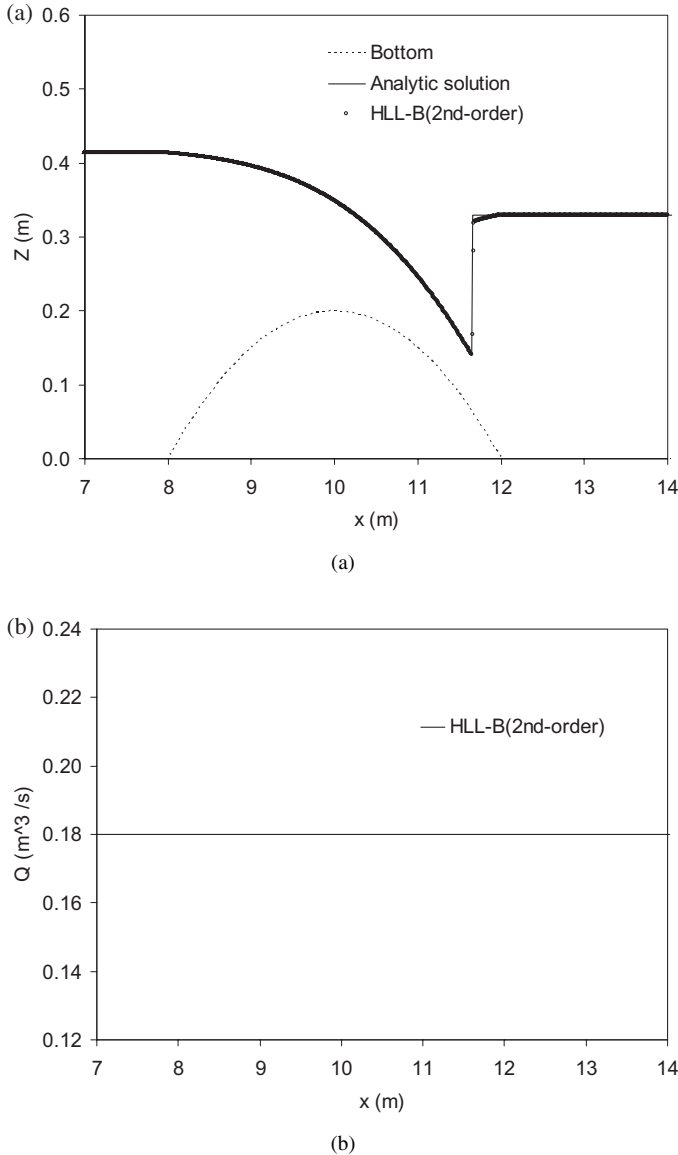

Figure 7 Comparison of numerical solutions with analytic solutions for the test case of steady flow over a bump with hydraulic jump (grid size $\Delta x = 0.1\,\text{m}$) : (a) water level; (b) discharge predicted by HLL-B schemes; and (c) discharge predicted by HLL-A schemes.

test case further demonstrate that the HLL-B scheme can accurately predict the discharge even in the presence of hydraulic jumps. Figure 7(c) shows the solution of discharge from the HLL-A schemes does not converge at the exact solution over several cells adjacent to the hydraulic jump, as the solutions from many other schemes (e.g., Vazquez-Cendon, 1999; Hubbard and Garcia-Navarro, 2000; Zhou *et al.*, 2001; Xu, 2002; Delis, 2003; Rogers *et al.*, 2003).

To investigate the effect of grid size on numerical solutions and whether they converge to the exact solutions as $\Delta x \to 0$, an additional calculation has been performed using $\Delta x = 0.01$ m. The numerical solution of water level is shown in Fig. 8(a). Comparisons between Fig. 7(a) and Fig. 8(a) show that reducing grid size can significantly improve the accuracy of numerical solution of water depth. The predicted water depth using $\Delta x = 0.01$ m is in very good agreement with the analytic solution, except in a very small area behind the hydraulic jump where the model slightly underpredicts the water level. Fig. 8 (b) also demonstrates that

the numerical solution of discharge using $\Delta x = 0.01$m and the analytic solution are an excellent match.

To further demonstrate the convergence of the numerical scheme, let us consider the test case of a subcritical steady flow over a bump, in which a unit discharge of 4.42 m²/s was imposed at the upstream boundary and water depth at downstream boundary was specified as 2.0 m. In the computation, $\Delta x = 0.1$ m and $\Delta t = 0.002$ s were used. The numerical result after reaching the steady state is compared with analytic solution in Fig. 9 and an excellent agreement between both is observed.

5.5 Wave interactions

In this section, we examine the scheme's ability to capture the wave interactions using two examples. Let us consider a 1210-m-long channel with solid boundaries at both ends. The channel is assumed to be horizontal and frictionless. Two dams are located at $x = 400$ m and $x = 810$ m, respectively, where x is the distance from the left end of the channel. In the first example, the initial water surface is assumed to be 10 m (400 m $\leq x \leq$ 810 m) and 2 m (other computational domain), respectively, see the picture of $t = 0$ s in Fig. 10(a). In the computation, $\Delta x = 10$ m and $\Delta t = 0.1$ s were used. The results at different times obtained by HLL-B (second-order) scheme are presented in Fig. 10(a). After the dam failure, two surges traveling in opposite directions are formed. Meanwhile, two depression waves are produced and move toward to the middle of the channel. At the middle part of the channel, a depression-on-depression interaction occurs. From Fig. 10(a), reasonable and symmetric solutions are observed.

In the second example, the initial water surface is assumed to be 2 m (400 m $\leq x \leq$ 810 m) and 10 m (rest of the computational domain), respectively, see the picture of $t = 0$ s in Fig. 10(b). The results at different times obtained by HLL-B (second-order) scheme are presented in Fig. 10(b). After the dam failure, two surges are produced and move toward to the middle of the channel. At $t = 30$ s, two surges has impinged each other

(a)

(b)

Figure 8   Comparison of numerical solutions with analytic solutions for the test case of steady flow over a bump with hydraulic jump (grid size $\Delta x = 0.01$ m) : (a) water level and (b) discharge.
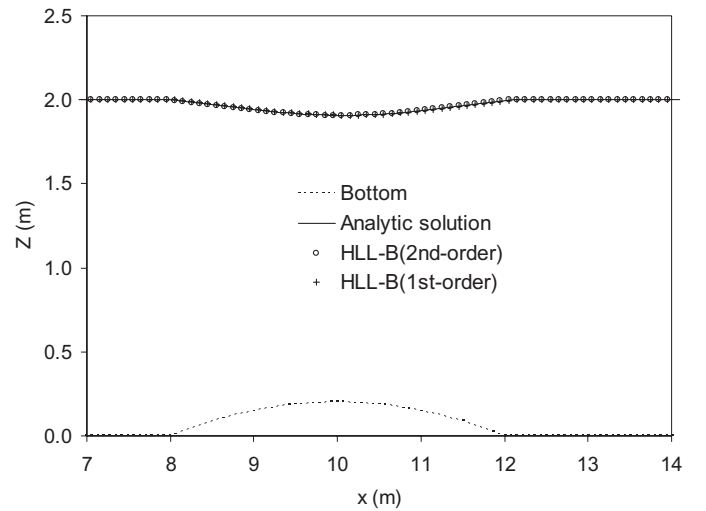

Figure 9   Comparison of numerical solutions of surface water level with the analytic solution for the test case of steady flow over a bump (subcritical flow).
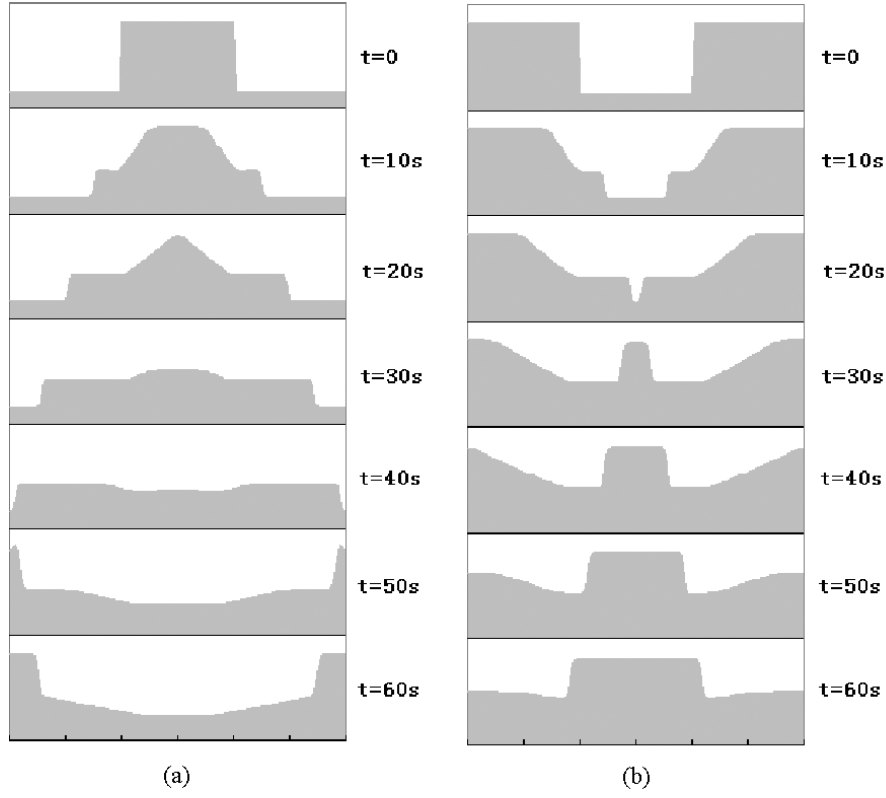
Figure 10   Numerical solutions of wave interactions: (a) depression-on-depression interaction and (b) shock-on-shock interaction.

and a shock-on-shock interaction occurs. Figure 10(b) shows that the scheme can correctly capture the shock-on-shock interaction and provide reasonable and symmetric solutions.

5.6   Tidal flow in an open channel

This test example was proposed by Bermudez and Vazquez (1994) and used by several other researchers (e.g., Xu, 2002). The bed elevation is defined by

$$Z_b(x) = 10 + \frac{40x}{L} + 10 \sin\left[\pi\left(\frac{4x}{L} - \frac{1}{2}\right)\right]$$

where L (= 14,000 m) is the channel length. At the initial time, water surface level $Z = 60.5$ m and velocity $V = 0$ m/s over the entire channel. The boundary conditions are

$$Z(0, t) = 64.5 - 4.0 \sin\left[\pi\left(\frac{4t}{86,400} + \frac{1}{2}\right)\right]$$

$$Q(L, t) = 0.0$$

An approximate solution can be written as (Bermudez and Vazquez, 1994):

$$Z(x, t) = 64.5 - 4.0 \sin\left[\pi\left(\frac{4t}{86,400} + \frac{1}{2}\right)\right]$$

and

$$V(x, t) = \frac{(x - L)\pi}{5400h(x, t)} \cos\left[\pi\left(\frac{4t}{86,400} + \frac{1}{2}\right)\right]$$

The numerical results from the HLL-B schemes at $t = 7552.13$ s with $\Delta x = 280$ m are presented in Figs. 11 and 12. It is observed that both first-order and second-order schemes are capable of accurately predicting water surface level and flow velocity.

5.7   Wave propagation

This test problem, proposed by LeVeque (1998), is selected to test numerical scheme's ability to capture short wave propagation in the shallow water. Consider a 1-m-long channel with rectangular cross-section, which is assumed to be horizontal and frictionless. The bed elevation is defined as

$$Z_b(x) = \begin{cases} 0.25(\cos(\pi(x - 0.5)/0.1) + 1.0) \\ \qquad\qquad\qquad \text{for} \quad |x - 0.5| \le 0.1 \\ 0 \quad \text{else} \end{cases}$$
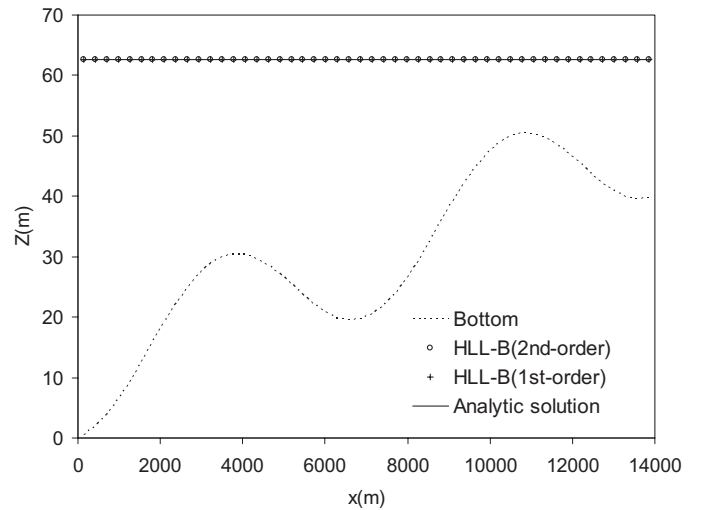

Figure 11   Comparison of numerical solutions of surface water level with the analytic solution for the unsteady channel flow problem.
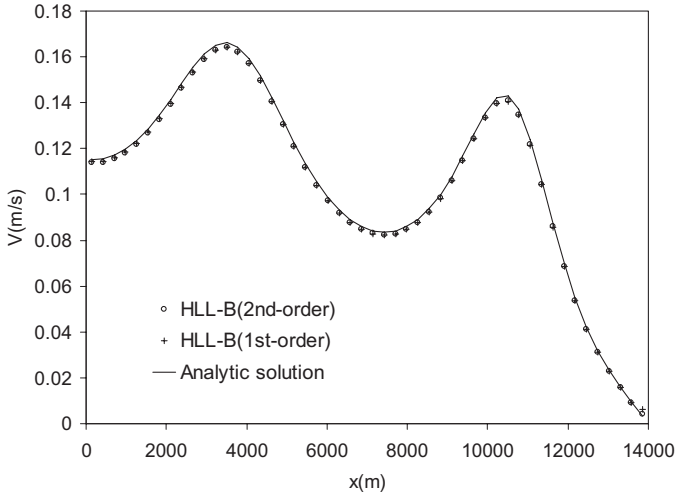
Figure 12   Comparison of numerical solutions of velocity with the analytic solution for the unsteady channel flow problem.
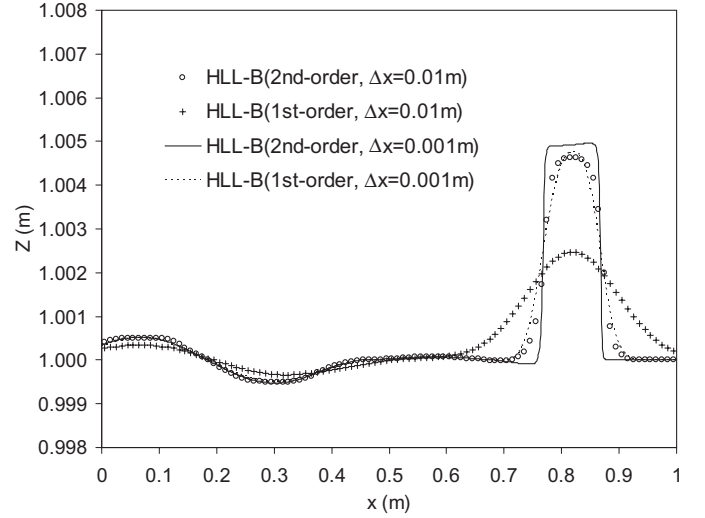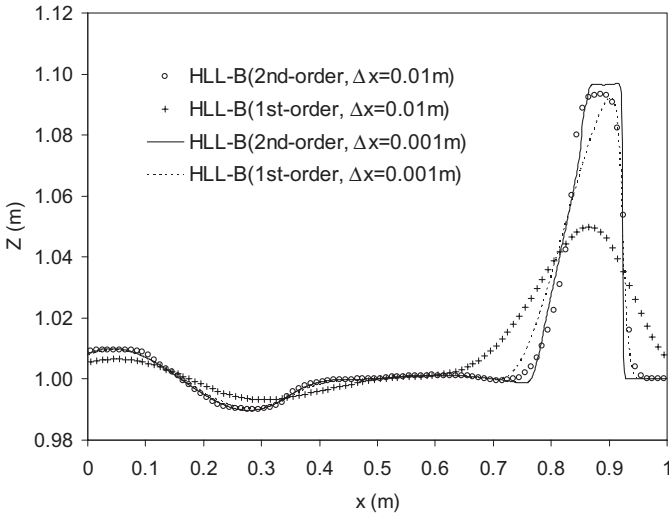

Figure 13   Numerical solutions of surface water level for the wave propagation problem with initial wave height $\varepsilon = 0.2$ m.

The initial water is stationary and the water surface level is defined as

$$Z(x) = \begin{cases} 1.0 + \varepsilon & \text{for } 0.1 \leq x \leq 0.2 \\ 1.0 & \text{else} \end{cases}$$

where ε is the initial wave height. The two cases with $\varepsilon = 0.2$ and 0.01 m were calculated using both first-order and second-order HLL-B schemes. The grid size $\Delta x = 0.001$ and 0.01 m were used, respectively. The gravitational acceleration $g = 1.0$ m/s^2. The predicted water surface level at $t = 0.7$ s are presented in Fig. 13 for the case with $\varepsilon = 0.2$ and Fig. 14 for the case with $\varepsilon = 0.01$. In both the cases the solutions obtained by the second-order HLL-B scheme are in very good agreement with those from other schemes (e.g., LeVeque, 1998; Xu, 2002; Delis, 2003). This illustrates that the second-order HLL-B scheme can satisfactorily reproduce wave propagation and the effect of uneven bed topography, even in the case of very small perturbation. The results also

Figure 14   Numerical solutions of surface water level for the wave propagation problem with initial wave height $\varepsilon = 0.01$ m.

show that the first-order HLL-B scheme has significant numerical diffusion, which causes the predicted wave peaks lower very quickly, especially in the case of coarse grid.

6   Conclusions

A numerical scheme for one-dimensional open channel flows has been developed based on several new techniques, including: (1) adopting the form of the Saint Venant equations that include both gravity and pressure in one source term; (2) using water surface level as one of the primitive variables, in stead of cross-sectional area; (3) defining discharge at interface and evaluating it according to the flux obtained by the HLL Riemann solver and (4) estimating water surface gradient based on linearly reconstructed data in the second-order scheme. The performance of the resulting HLL-B schemes is evaluated by means of theoretical analysis and various test examples, including ideal dam-break flows with dry and wet bed, hydraulic jump, steady flow over bump with hydraulic jump, wave interactions, tidal flow in an open channel, and wave propagation. It is clearly demonstrated that both the first-order and the second-order HLL-B schemes have excellent numerical balance. The new schemes can successfully eliminate the problem of failure to satisfy mass conservation when a hydraulic jump is present.

The numerical tests further illustrate that the second-order HLL-B scheme is capable of satisfactorily predicting all these one-dimensional open channel flows, which may includes discontinuities, transcritical flows, wave interactions, and flows with irregular geometry and initial dry bed. The second-order HLL-B scheme may produce very diffusive solutions in some severe test cases, such as the wave propagation problem. However, in the cases where the spatial variations of flow characteristics are relatively smooth, for example, the hydraulic jump and the tidal flow problems, the first-order scheme can work as well as the second-order schemes.

Appendix

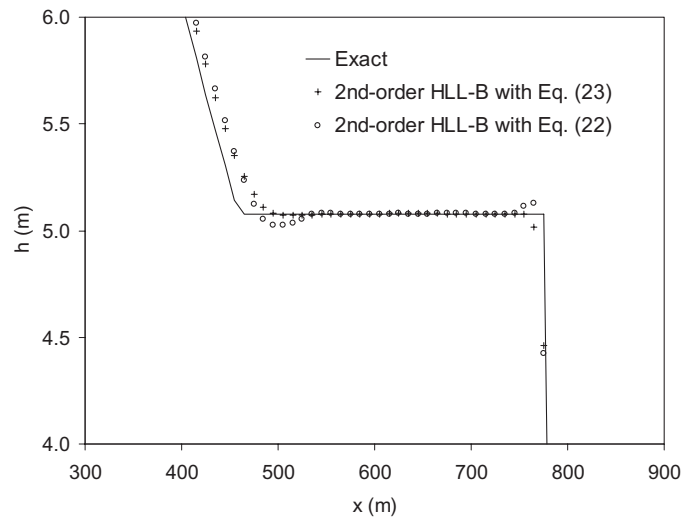Comparisons between the numerical results from the second-order HLL-B scheme with Eqs (22) and (23) are made by means of the idealized dam-break problem in a rectangular channel with wet bed. The computational conditions are described in the Section 5.2. The results of water depth, discharge, and velocity are presented in Figs A-1–A-3, respectively. From these figures, it is clearly observed that using Eq. (22) produces non-monotone solutions near the discontinuities and significant improvement in all these numerical solutions can be made by using Eq. (23).

In Figs A-4, A-5, A-6, the results from the second-order HLL-B scheme with non-uniform grid ($\Delta x_i = 8, 2, 8, 2, \ldots$, for $i = 1, 2, 3, 4, \ldots$) are compared with those computed using the uniform grid with the same total number of cells ($\Delta x = 5$ m). The water surface gradient is estimated using Eq. (23) in both calculations with uniform and non-uniform grid. The results show that the second-order HLL-B scheme with Eq. (23) can perform well even in the case of non-uniform grid.

Figure A1   Comparisons between numerical solutions of water depth from the second-order HLL-B scheme with Eqs (22) and (23).

Figure A3   Comparisons between numerical solutions of velocity from the second-order HLL-B scheme with Eqs (22) and (23).
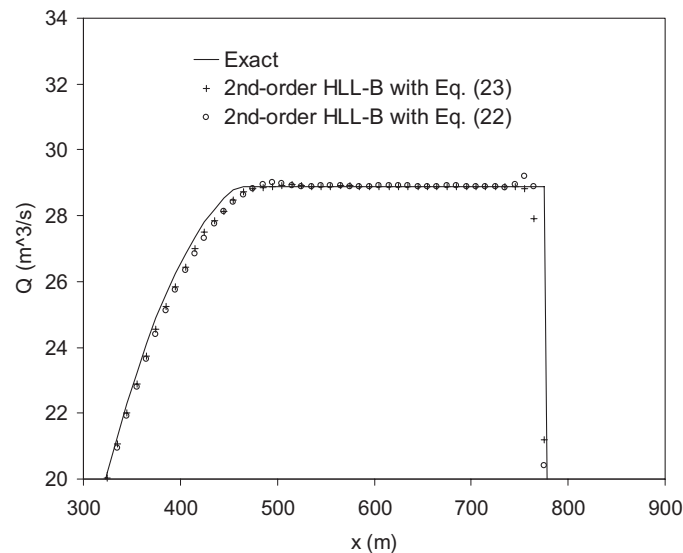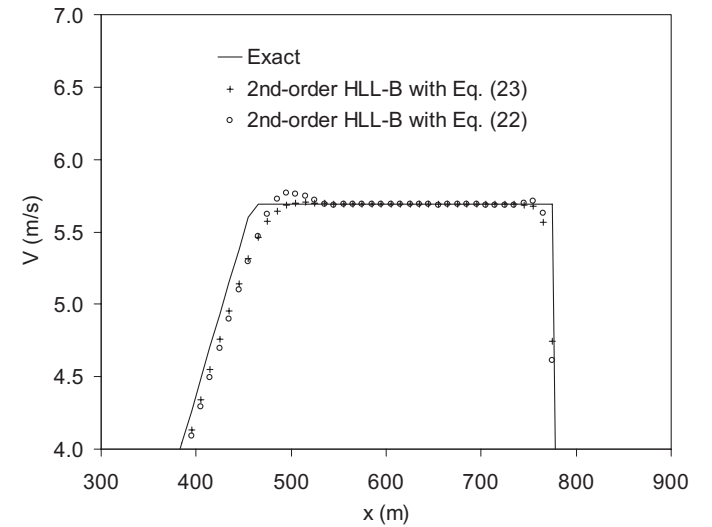

Figure A2   Comparisons between numerical solutions of discharge from the second-order HLL-B scheme with Eqs (22) and (23).
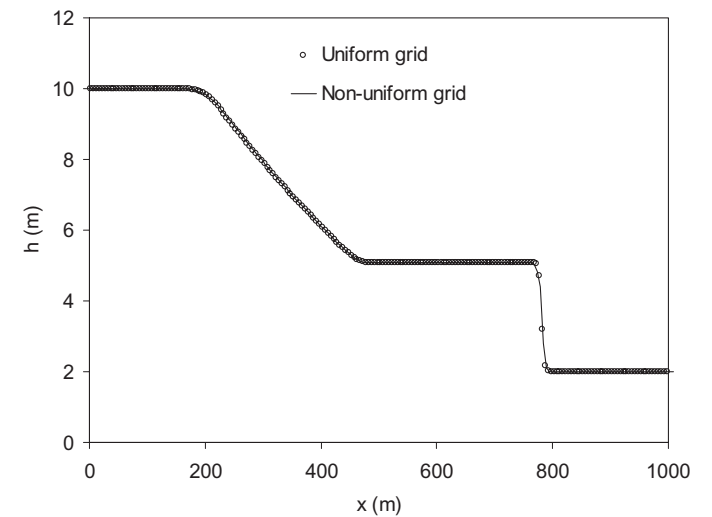

Figure A4   Comparisons between numerical solutions of water depth from the second-order HLL-B scheme with uniform and non-uniform grids.
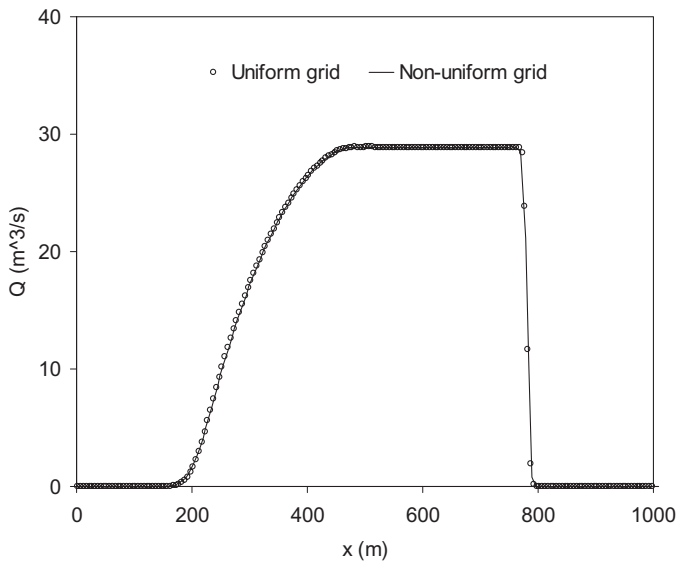
Figure A5 Comparisons between numerical solutions of discharge from the second-order HLL-B scheme with uniform and non-uniform grids.
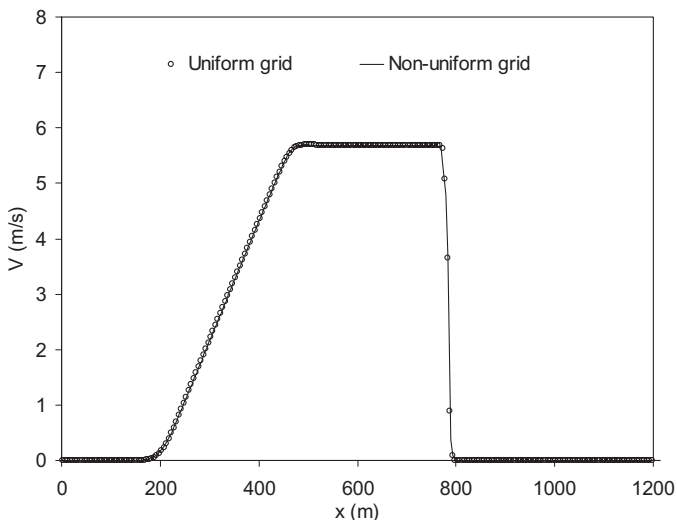

Figure A6 Comparisons between numerical solutions of velocity from the second-order HLL-B scheme with uniform and non-uniform grids.

References

1. BERMUDEZ, A. and VAZQUEZ, M.E. (1994). "Upwind Methods for Hyperbolic Conservation Laws with Source Terms". *Comput. Fluid.* 23(8), 1049–1071.

2. BURGUETE, J. and GARCIA-NAVARRO, P. (2001). "Efficient Construction of High-Resolution TVD Conservative Schemes for Equations with Source Terms: Application to Shallow Water Flows". *Int. J. Numer. Meth. Fluid.* 37, 209–248.

3. CHOW, V.T. (1959). "Open Channel Hydraulics". McGraw-Hill, New York, USA.

4. CUNGE, J.A., HOLLY, F.M. Jr. and VERWEY, A. (1980). *Practical Aspects of Computational River Hydraulics*. Pitman Publishing Limited, London.

5. DELIS, A.I. (2002). "Higher Order Numerical Methods Evaluation for the Computation of One Dimensional Free Surface Shallow Water Flows". *Intern. J. Comput. Engrg. Sci.* 3(1), 13–55.

6. DELIS, A.I. (2003). "Improved Application of the HLLE Riemann Solver for the Shallow Water Equations with Source Terms". *Commun. Numer. Meth. Engrg.* 19, 59–83.

7. FRACCAROLLO, L. and TORO, E.F. (1995). "Experimental and Numerical Assessment of the Shallow Water Model for Two-Dimensional Dam-Break Type Problems". *J. Hydraul. Res.* 33(6), 843–864.

8. GARCIA-NAVARRO, P. and VAZQUEZ-CENDON, M.E. (2000). "On Numerical Treatment of the Source Terms in the Shallow Water Equations". *Comput. & Fluid.* 29, 951–979.

9. GARCIA-NAVARRO, P., ALCRUDO, F. and SAVIRON, J.M. (1992). "1-D Open Channel Flow Simulation Using TVD-MacCormack Scheme". *J. Hydraul. Engrg.* 118(10), 1359–1372.

10. GHARANGIK, A.M. and CHAUDHRY, M.H. (1991). "Numerical Simulation of Hydraulic Jump". *J. Hydraul. Engrg.* 117(9), 1195–1211.

11. GODUNOV, S.K. (1959). "Finite Difference Method for Numerical Computation of Discontinuous Solutions of the Equations of Fluid Dynamics". *Math. Sbonik* 47(3), 271–306 (in Russian).

12. GRAF, W.H. and ALTINAKAR, M.S. (1998). *Fluvial Hydraulics*. John Wiley & Sons Ltd, England.

13. HARTEN, A., LAX, P.D. and VAN LEER, B. (1983). "On Upstream Differencing and Godunov-type Schemes for Hyperbolic Conservation Laws". *SIAM Rev.* 25(1), 35–61.

14. HENDERSON, F.M. (1966). "Open Channel Flow". McGraw Hill Publishing, New York.

15. HUBBARD, M and GARCIA-NAVARRO, P. (2000). "Flux Difference Splitting and the Balancing of Source Terms and Flux Gradients". *J. Comput. Phys.* 165, 89–25.

16. JIN, M. and FREAD, D.L. (1997). "Dynamic Flood Routine with Explicit and Implicit Numerical Solution Schemes". *J. Hydraul. Engrg.* 123(3), 166–173.

17. LEVEQUE, R. J. (1998). "Balancing Source Terms and Flux Gradients in High-Resolution Godunov Methods: The Quasi-Steady Wave-Propagation Algorithm". *J. Comput. Phys.* 146, 346–365.

18. NUJIC, M. (1995). "Efficient Implementation of Non-oscillatory Schemes for the Computation of Free-Surface Flows". *J. Hydraul. Res.* 33(1), 100–111.

19. ROGERS, B.D., BORTHWICK, A.G.L. and TAYLOR, P. H. (2003). "Mathematical Balancing of Flux Gradient and Source Terms Prior to Using Roe's Approximate Riemann Solver". *J. Comput. Phys.* 192, 422–451.

20. SANDERS, B.F. (2001). "High-Resolution and Non-oscillatory Solution of the St. Venant Equations in Non-rectangular and Non-prismatic Channels". *J. Hydraul. Res.* 39(3), 321–330.

21. SOARES FRAZAO, S. and ZECH, Y. (1999). "Computation of Extreme Flood Flow Through the Toce Valley". *Proceedings of the 3rd CADAM Workshop*, Milan, Italy.

22. SOARES FRAZAO S. and ZECH, Y. (2002). "Dam Break in Channels with 90° Bend". *J. Hydraul Engrg.* 128(11), 956–968.

23. TORO, E.F. (2001). *Shock-Capturing Methods for Free-Surface Shallow Flows*. John Wiley & Sons Ltd.

24. VALIANI, A., CALEFfi, V. and ZANNI, A. (2002). "Case Study: Malpasset Dam-Break Simulation Using a Two-Dimensional Finite Volume Method". *J. Hydraul. Engrg.* 128(5), 460–472.

25. VAZQUEZ-CENDON, M.E. (1999). "Improved Treatment of Source Terms in Upwind Schemes for Shallow Water Equations in Channels with Irregular Geometry". *J. Comput. Phys.* 148, 497–526.

26. XU, K. (2002). "A Well-Balanced Gas-Kinteic Scheme for the Shallow Water Equations with Source Terms". *J. Comput. Phys.* 178, 533–562.

27. YING, X., KHAN, A. and WANG, S.S.Y. (2004). "Upwind Conservative Scheme for the Saint Venant Equation". *J. Hydraul. Engrg.* 130(10), 977–987.

28. ZHOU, J.G., CAUSON, D.M., MINGHAM, C.G. and INGRAM, D.M. (2001). "The Surface Gradient Method for the Treatment of Source Terms in the Shallow-Water Equations". *J. Comput. Phys.* 168, 1–25.

29. ZOPPOU, C. and ROBERTS, S. (2003). "Explicit Schemes for Dam-Break Simulations". *J. Hydraul. Engrg.* 129(1), 11–34.